Journal of Photochemistry & Photobiology A: Chemistry 384 (2019) 112048

Contents lists available at ScienceDirect

Journal of Photochemistry & Photobiology A: Chemistry

journal homepage: www.elsevier.com/locate/jphotochem

Excited-state investigations of *meso*-mono-substituted-(amino-ferrocenyl) porphyrins: Experimental and theoretical approaches

Leandro H.Z. Cocca[a], Lucas F. Sciuti[a,b], Lucas B. Menezes[c], Mateus H. Köhler[d], Andressa C. Bevilacqua[d], Paulo C. Piquini[d], Bernardo A. Iglesias[c,*], Leonardo de Boni[a,b,**]

[a] Instituto de Física de São Carlos, Universidade de São Paulo, São Carlos, SP, Brazil
[b] Escola de Engenharia de São Carlos, Universidade de São Paulo, São Carlos, SP, Brazil
[c] Laboratório de Bioinorgânica e Materiais Porfirínicos, Departamento de Química, Universidade Federal de Santa Maria – UFSM, 97105-900 Santa Maria, RS, Brazil
[d] Departamento de Física, Universidade Federal de Santa Maria – UFSM, 97105-900 Santa Maria, RS, Brazil

ARTICLE INFO

Keywords:
Porphyrins
Ferrocenyl derivatives
Photophysical properties

ABSTRACT

The spectroscopic study and characterization of mono-(amino-ferrocenyl) porphyrins has increased during the last years. These molecules can be synthesized in such a way that their linear and nonlinear optical parameters are modulated, opening the possibility for new applications, such as in photodynamic therapy. In this work, we perform a spectroscopic characterization of a group of five free-base porphyrins, three of them having a C_6F_4 group attached to an amino-ferrocene moiety through a $-NH(CH_2)_nNH-$ spacer, in which n = 2, 4 or 6. These three molecules differ by the size of the aliphatic chain. For this study, we employ linear as well as nonlinear optical spectroscopic techniques, such as the Z-Scan and time resolved fluorescence. Decay times, absorption cross-sections and quantum yields were determined, and the results suggest that, for this group of molecules, the differences in the aliphatic chain sizes joining the ferrocenyl unit to the C_6F_4 group at the *para*-position aryl ring do not influence significantly the optical parameters. Further, DFT calculations confirm that the UV–vis absorbance and the associated electronic transitions are not affected by the size of the aliphatic chain spacers. Thus, it is possible to state that these molecules can interact with biomolecules through the ferrocene unit while keeping their optical properties unchanged.

1. Introduction

The photophysical and photochemical spectroscopic characterization of materials constituted by organic macrocycles, such as porphyrins, has gained great interest in the last years. The flexibility to synthesize these materials allows the modeling of their photophysical optical parameters through the insertion of different lateral chemical structures or different metallic ions in the macrocycle [1,2]. Porphyrins are constituted by an organic macrocycle containing π-conjugation, which provides considerable nonlinear optical effects [3,4]. In addition, this class of materials also exhibits considerable linear absorption in the UV–vis region [5,6]. These characteristics make porphyrins good candidates for several applications, such as for optical limiters [7–10], saturable absorbers [11], and organic solar cells [12,13].

Porphyrins are extensively used in photodynamic therapy (PDT) [14] because of the presence of intersystem crossing process. As it is known, high intersystem crossing quantum yields of porphyrins (normally observed in free-based porphyrins) makes this family of molecules desirable for PDT [15,16]. For a molecule to be considered as a good photosensitizer, it is necessary to present a considerable yield of triplet state formation, that is, the electrons of the molecule must present a considerable intersystem crossing (a singlet to triplet non-radiative transition) at the excited state. Also, triplet state formation can be induced by one- or two-photon [16], increasing the use of this molecule as photosensitizer due to the penetrability of light in the tissue by using wavelengths that are within the spectral region called “therapeutic window” [16].

Porphyrin molecules are being synthesized and characterized for the purpose of drug development due to the fact they interact with biomolecules such as DNA [17–22]. Several studies have been carried out with porphyrins bounded to a redox group. Such insertion offers a mean to reinforce their electronic interactions with biological molecules, and to their use in biomedical applications [23–25]. Generally, the redox group is attached directly to the porphyrin ring or through spacer

* Corresponding author.
** Corresponding author at: Instituto de Física de São Carlos, Universidade de São Paulo, São Carlos, SP, Brazil.
E-mail addresses: bernardopgq@gmail.com (B.A. Iglesias), deboni@ifsc.usp.br (L. de Boni).

https://doi.org/10.1016/j.jphotochem.2019.112048
Received 24 May 2019; Received in revised form 9 August 2019; Accepted 22 August 2019
Available online 23 August 2019

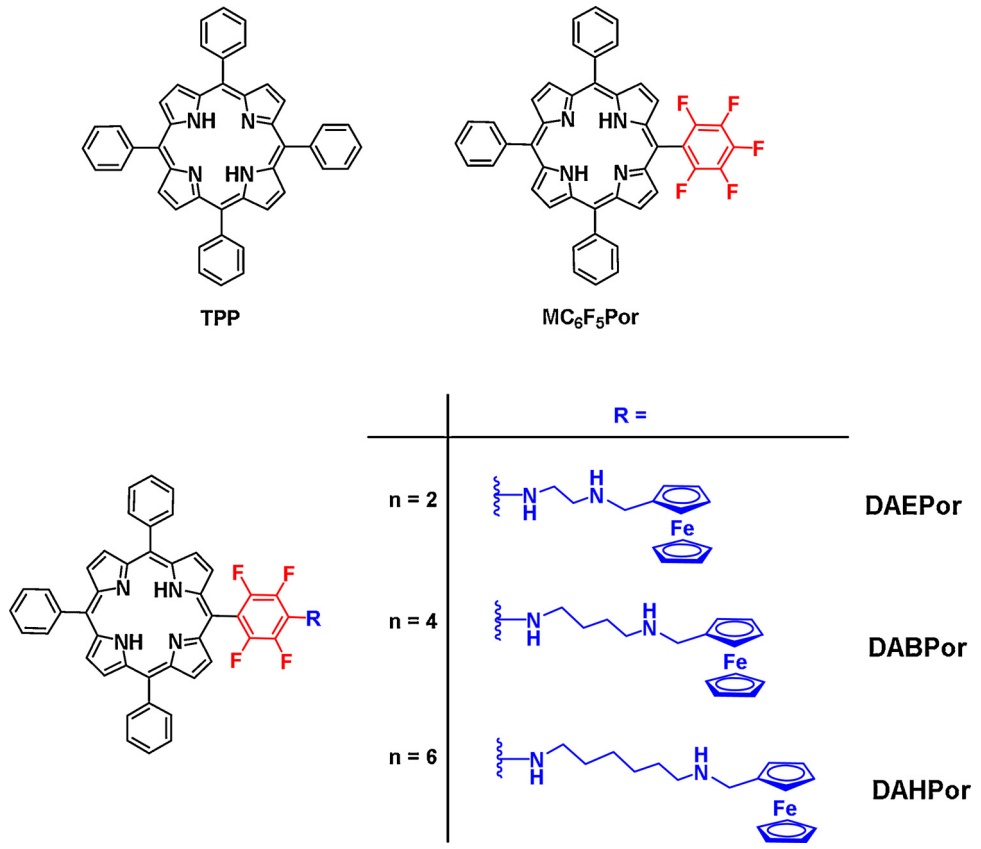

Fig. 1. Representative molecular structures of *meso*-(amino-ferrocenyl)porphyrins studied in this work.

groups, for example, multi-fluorinated, amino or hydroxyphenyl groups. The insertion of a redox group into the porphyrin ring may alter the molecular spectroscopic properties. On the other hand, the spectroscopic parameters can be preserved, due to the presence of spacer groups between the redox group and the porphyrin ring. A group that can be inserted peripherally to the porphyrin ring is the ferrocene group, which is a strong electron acceptor. The electronic structure and electrochemical behavior of ferrocene-porphyrins have been widely studied [26–28].

In this contribution, we investigate the excited state optical properties taking into account contributions from singlet and triplet states population dynamics. Excited state absorption properties as well as the intersystem crossing mechanism rates were evaluated for a set of three ferrocene free-based porphyrins: *meso-5*-(4-aminoethylferrocenyltetrafluorophenyl)-10,15,20-tri(phenyl)porphyrin (**DAEPor**), *meso-5*-(4-aminobutylferrocenyltetrafluorophenyl)-10,15,20-tri(phenyl)porphyrin (**DABPor**) and *meso-5*-(4-aminohexylferrocenyltetrafluorophenyl)-10,15,20-tri(phenyl)porphyrin (**DAHPor**), as shown in Fig. 1. The study was performed comparing the experimental/theoretical optical properties of the ferrocene porphyrins with the *meso*-tetra(phenyl)porphyrin (**TPP**) and *meso*-5-(pentafluorophenyl)-10,15,20-tri(phenyl)porphyrin (**MC_6F_5Por**), respectively, by using linear and nonlinear spectroscopy experiments. Decay times, excited state absorption processes and quantum yields were determined for the excited singlet and triplet states. The obtained results shown that ferrocene free-based porphyrins can be used as optical limiters for some range of wavelengths either as saturable absorber for other wavelengths. Nevertheless, the considerable intersystem crossing quantum yield observed, which was evaluated to be around 40%, turn these ferrocene porphyrins also possible photosensitizers to be used in PDT. In addition, as important result of this work, it was observed that the length of the aliphatic chain unchanged significantly the photophysical properties.

2. Experimental

2.1. Materials

Commercially available reagents were used in the present investigations. Analytical reagent grade solvents were used for synthesis of porphyrin and for column chromatography. Anhydrous solvents for photophysical measurements were purchase by Sigma-Aldrich® Company.

2.2. Synthesis

Porphyrins **MC_6F_5Por**, **DAEPor** and **DABPor** were synthesized and fully characterized according to a previously described method by Auras and co-workers 18.

2.2.1. Synthesis of meso-5-(4-aminohexylferrocenyltetrafluorophenyl)-10,15,20-tri(phenyl)porphyrin derivative (DAHPor)

Porphyrin **MC_6F_5Por** (200 mg, 0.284 mmol, 1.0 equiv.) and the amino-hexyl ferrocene derivative 18 (87 mg, 0.340 mmol, 1.2 equiv.) were dissolved in DMSO (10 mL) and stirred at 50 °C for 4 h. After this period, water and chloroform were added and the organic layer was separated and dried with sodium sulfate. The solvent was evaporated, and the residue was purified by silica-gel column chromatography using DCM/*n*-hexane (1:3, v/v) as eluent. Then, the resulting residue was purified by preparative silica-gel TLC plates using a mixture of DCM/MeOH (90:10, v/v) to afford pure dark purple solid porphyrin **DAHPor**. **Spectroscopic data for porphyrin (DAHPor)**: Dark-purple solid (98 mg, 0.099 mmol, 35% yield). M.p. > 300 °C (decomp.). ^{1}H NMR (600 MHz, $CDCl_3$): δ = −2.75 (bs, 2H, inner NH), 1.26 (m, 3H, $H_{aliphat}$), 1.53 (m, 4H, $H_{aliphat}$), 3.65–4.27 (m, 11H, $H_{aliphat}$ and *FeCp*), 7.77 (m, 9H, *m*- and *p-Ph*), 8.22 (d, 6H, *J* = 7.2 Hz, *o-Ph*), 8.84–8.91 (m, 8H, *β*-H). ^{13}C NMR (125 MHz, $CDCl_3$): δ = 18.4, 26.9, 30.9, 45.9, 58.4, 68.2,

69.3, 120.4, 121.4, 126.7, 127.7, 134.5, 141.9, 142.0. ^{19}F NMR (565 MHz, $CDCl_3$): δ = -161.13 (d, J_1 = 16.9, F_{ortho}), -140.73 (d, J_1 = 16.9, F_{meta}). FT-IR (KBr pellets, cm^{-1}): 3438 (ν_{N-H}), 2919 (ν_{C-H}), 2849 ($\nu_{C=C}$), 1654/1470 ($\nu_{C=N}$), 964 (ν_{C-N}) and 799 (δ_{C-H}). Anal. calcd. for $C_{61}H_{50}F_4FeN_6$: C, 73.34%; H, 5.05%; N, 8.41%. Found: C, 73.37%; H, 5.06%; N, 8.42%. HRMS-ESI, $[M+H]^+$: m/z 999.3463 (calcd for $C_{61}H_{50}F_4FeN_6$: 998.3383).

Spectral data such as FT-IR, HRMS-ESI and NMR spectra of **DAHPor** porphyrin are presented in Supplementary information (Figs. S1–S5).

2.3. Methods and instrumentation

The ferrocene-porphyrins spectra at the UV–vis region (about 200–900 nm) were obtained using the SHIMADZU UV-1800 spectrophotometer. The ferrocenyl-porphyrins were dissolved in dichloromethane (DCM) in 10^{-4} mol L^{-1}. It is important to mention that the measurements were performed at a 1.0 mm optical path length fused silica cuvette. For the determination of the fluorescence spectra, we employed a fluorimeter HITACHI F7000, where the molecules were dissolved at a concentration of about 10^{-6} mol L^{-1} to avoid fluorescence reabsorption, in a 1.0 cm optical path length fused silica cuvette. Elemental CHN% analysis was performed using a Perkin-Elmer CHN% 2400e equipment (São Paulo). Porphyrin was analyzed with a high--resolution electrospray ionization mass spectrometry (HRMS-ESI) instrument (microTOF QII, Bruker Daltonics, Billerica, MA). Mass spectra were obtained with MeOH solutions of concentration around 500 ppb with a flow of 180 μl min^{-1} and capillary of 3000–4500 V. ^{1}H, ^{13}C and ^{19}F NMR spectra were performed with a Bruker Avance III spectrometer at 600 (^{1}H), 125 (^{13}C) and 565 (^{19}F) MHz. $CDCl_3$ was used as solvent and TMS as the internal reference. The chemical shifts are expressed in δ (ppm) and coupling constants (J) are given in Hertz (Hz). Infrared analyses (FT-IR) were performed on a Perkin Elmer FTIR 100 spectrophotometer, in the 4000–400 cm^{-1} region, using KBr pellets (spectroscopy grade).

2.4. Theoretical TD-DFT calculations

The electronic and structural properties of the compounds were studied using the Density Functional Theory (DFT), as implemented in the Gaussian 09 code [29]. The ground state geometrical structures were optimized (energy minimization) employing conjugated gradient techniques. The absorption spectra were determined using the time-dependent DFT (TD-DFT). No optimization of the excited states was performed. The long-range corrected CAM-B3LYP [30] functional was used to describe the exchange and correlation potentials. The 6-31G+(d,p) basis set [31] was used in all calculations. Previous simulations have demonstrated the accuracy of this procedure in describing the optical absorbance of peripheral-substituted macrocycles [32]. The polarizable continuum model (PCM) was employed to calculate the molecular properties in dichloromethane [33].

2.5. Fluorescence quantum yield

The ability of ferrocene porphyrin molecules to decay from the first excited singlet state (S_1) to the ground singlet state (S_0) via emission of radiation can be determined by measuring the fluorescence quantum yield (ϕ_f). For the ϕ_f determination we used the well-known Brouwer method [34], which makes use of a molecule of known fluorescence quantum yield, applying to the following equation:

$$\phi_f = \phi_f^{ref} \cdot \frac{\int_{\lambda_0}^{\lambda_f} F(\lambda)\, d\lambda}{\int_{\lambda_0}^{\lambda_f} F_{ref}(\lambda)\, d\lambda} \cdot \frac{f_{ref}}{f} \cdot \frac{n^2}{n_{ref}^2}, \quad (1)$$

in which ϕ_f^{ref} is the previously known fluorescence quantum yield (8% for hematoporphyrin dissolved in dimethyl sulfoxide (DMSO) [35], and the *n's* are the solvent's refractive indexes. $f = 1 - 10^{-A(\lambda_{ex})}$ is the quantity of absorbed light, in which A is the absorbance of the sample at the excitation wavelength (λ_{ex}), taken as the same for both compounds. Finally, $F(\lambda)$ ´s are the fluorescence spectra integrated over all emission range. Molecules were dissolved to a concentration of about 10^{-6} mol L^{-1}, and the $F(\lambda)$ measurements were obtained through a HITACHI F7000 fluorimeter.

2.6. Time resolved fluorescence

Fluorescence lifetime (τ_f) was determined using the time resolved fluorescence technique by using the doubled frequency (532 nm) of a Nd:YAG Q-Switched mode-locked laser operating at 1064 nm, with pulses of 100 ps and 100 Hz of repetition rate. The laser pulses strike the porphyrin molecule promoting the electrons from the ground singlet state to the first excited singlet state. After a characteristic time (of the order of 10^{-9} s, for these molecules), some electrons return to the ground state by fluorescent emission. This fluorescence is collected perpendicular to the excitation beam and using a 532 nm filter to avoid any interference of this beam. The fluorescence signal, $I(t)$, is registered by a 1 ns temporal resolution silicon photodetector and, through an exponential fitting ($I(t) = I_0 e^{-t/\tau_f}$) of the fluorescence curves, it was possible to determine τ_f. I_0 is the fluorescence intensity at time zero. The technique was calibrated with Rhodamine B dissolved in ethanol.

2.7. Single pulse and white light Z-scan techniques

In order to determine the first excited state absorption cross section at 532 nm ($\sigma_{1n}(532\,nm)$) and first excited state absorption cross section spectra ($\sigma_{1n}(\lambda)$), we used the Z-Scan by single pulse [36] and white light continuum Z-Scan techniques [37]. The single-pulse Z-Scan technique relies on monitoring the normalized transmittance (NT) from a sample as it is translated around a previously focused pulsed laser beam. The laser beam is derived from a double frequency (532 nm) Nd:YAG mode-locked and Q-Switched laser, with pulse of 100 ps and repetition rate of 100 Hz. The laser beam is focused by a 12 cm convergent lens. The normalized transmittance from the sample is captured by a 1.0 cm^2 PIN photodetector, in which the electric signal is amplified and averaged in a locking amplifier. The data are acquired by a homemade LabView program, which also controls the Z-Scan experiment.

For the determination of the excited state absorption cross section spectra from 450 up to 800 nm ($\sigma_{1n}(\lambda)$), we used the white light continuum Z-Scan technique, which employs Ti:Sapphire laser (CPA-2001 system from Clark-MXR Inc.) that is capable of generating pulses at 775 nm, 150 fs time duration with 1.0 kHz of repetition rate. This pulse passes an optical parametric amplifier (TOPAS Quantronix) which is tuned to generate pulses of 1100 nm with the same repetition rate and 120 fs pulsewidth. This pulse (1100 nm) crosses a 3.0 cm cuvette containing distilled water, where supercontinuum white light is generated (from 450 nm up to 800 nm). As in Z-Scan by single pulse, the material is translated around the supercontinuum white light (previously focalized by an 8.0 cm lens) and the normalized transmittance as a function of the Z position of the sample is monitored. Such transmittance is collected by a CCD spectrophotometer and the data is acquisitioned by a computer through a homemade LabView program.

2.8. Pulse train Z-Scan (PTZS) technique

In order to determine the triplet state characteristics (triplet state absorption cross section and intersystem crossing time, τ_{isc}), we used the Z-Scan by pulse train technique [38]. For this purpose, a doubled frequency (532 nm) mode-locked and Q-Switched Nd:YAG laser was used, working at repetition rate of 10 Hz. This configuration (Q-Switched and mode-locked) generates an envelope of approximately 300 ns time duration with approximately 30 pulses, each pulse with 100 ps and separated from each other by approximately 13 ns. Similarly, as in Z-

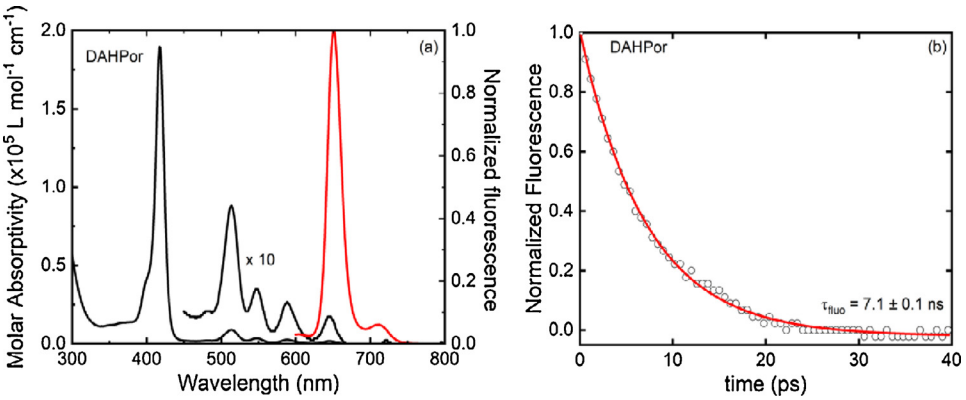

Fig. 2. Left: (a) Molar absorptivity in UV–vis region (black lines) and fluorescence emission (red line) for the **DAHPor** molecule using DCM as solvent. Right: (b) Fluorescence decay curve (black circles) and exponential fitting (red line) to fluorescence life time determination for the **DAHPor** porphyrin.

Scan by single pulse and Z-Scan by white light, the sample was translated around a focal region, and the optical transmittance was measured away from the focus and at the focus. Hence, it was possible to obtain the normalized transmittance. Such transmittance was collected by a 1.5 mm^2 fast photodetector with 1.0 ns temporal resolution. Data acquisition and sample translation were controlled through a homemade LabView program.

3. Results and discussion

3.1. Linear optical experiments

To begin with, we performed linear optical spectroscopy experiments. Through these experiments, we were able to determine molar absorptivity spectra, fluorescence emission spectra, fluorescence lifetimes, and fluorescence quantum yields. Fig. 2(a) shows the absorption bands of the **DAHPor** molecule dissolved in DCM (solid black line). It is possible to note a Soret band with a peak at approximately 400 nm and 4 Q-bands, with absorption peaks at approximately 510 nm, 550 nm, 590 nm and 640 nm. In addition to the molar absorptivity spectra, it is also possible to observe in Fig. 2(a) the fluorescence emission (for excitation wavelength at 510 nm) with a maximum peak at 650 nm (solid red line). Finally, Fig. 2(b) shows the fluorescence decay curve of **DAHPor** compound (circles), which was excited by a pulsed 100 ps laser beam at 532 nm. Through such a fluorescence curve, it was possible to trace an exponential fitting (solid line) and determine the fluorescence lifetime of about 7.1 ns.

It is important to mention here that the absorption spectrum (molar absorptivity), fluorescence spectrum, and the fluorescence time decay curve of the **DAHPor** show a very similar result for the other four porphyrins, which were described in a previous work 18. We noted, comparing such spectra, that there is no displacement in both Q-bands and the Soret band as the chemical structures are altered. Also, molar absorptivity values are not significantly changed for the **MC$_6$F$_5$Por**, **DAEPor**, **DABPor** and **DAHPor** molecules, with a little increase of about 1.2 times for **TPP**. These statements can be verified in Table 1.

Fluorescence quantum yield were calculated with Eq. (1) and using hematoporphyrin as the standard calibration compound. Integrating the fluorescence spectrum, $F(\lambda)$, and known the amount of light (f) that the sample absorb at the excitation wavelength, we were able to compare the samples with the standard. Through this methodology, the fluorescence quantum yields (ϕ_f) for all five porphyrins were calculated. These values are depicted in Table 1 together with other spectroscopic characteristics, such as the wavelength position of the Soret and Q-bands at UV–vis and the respective molar absorptivity values, inside parentheses. In addition, Table 1 presents the maximum emission wavelength (λ_{em}), which are almost not modified, and the fluorescence lifetimes (τ_f).

TPP molecule dissolved in DCM has the highest fluorescence quantum yield (2.4%), when compared to the other four porphyrins (**MC$_6$F$_5$Por**, **DAEPor**, **DABPor** and **DAHPor**). This can be understood due to the addition of the C_6F_4 group to the porphyrinic macrocycle. It is known that the addition of groups containing halogenic elements favors non-radiative decay (internal conversion), therefore, the quantum efficiency should be lower for porphyrins that contain halogens [39,40]. Additionally, we noted that there is no significant difference, considering the experimental error, in the ϕ_f values for **MC$_6$F$_5$Por**, **DAEPor**, **DABPor** and **DAHPor** porphyrins.

It is interesting to point out a small reduction in the lifetime for the three porphyrins containing ferrocene units. This behavior was also observed by Wu and co-workers [41] in BODIPY-type molecules containing ferrocene units. According to the authors, in the ground state, there is not significant interaction between the ferrocene and BODIPY moieties. However, upon irradiation, quenching in the fluorescence emission due to electron transfer mechanism from ferrocene moiety to the singlet state of BODIPY is observed for some BODIPY-types, with a conjugated bridge binding ferrocene moiety to the fluorophore. Also, the fluorescence lifetime is slightly affected by the chain bounding ferrocene and the BODIPY moiety [42].

In our case, considering only the molecules that have the ferrocene group bound to the C_6F_4 group through the aliphatic chain (**DAEPor**, **DABPor** and **DAHPor**), the fluorescence lifetimes are slightly altered as well. Comparing them, the shortest fluorescence lifetime is the one obtained for **DAEPor**, which has the shortest aliphatic chain length. For

Table 1
Absorption wavelength (λ_{abs}), molar absorptivity (ε), emission wavelength (λ_{em}), fluorescence quantum yield (ϕ_f) and fluorescence life time for all ferrocenyl-porphyrins samples.

Compound	λ_{abs}(nm) and ε($\times 10^5$ L mol^{-1} cm^{-1})	λ_{em} (nm)	ϕ_f (%)	τ_f (ns)
TPP	416 (1.8), 514 (0.08), 549 (0.03), 592 (0.02), 648 (0.02)	652	2.4 ± 0.3	8.8 ± 0.1
MC$_6$F$_5$Por	416 (1.5), 512 (0.07), 549 (0.02), 588 (0.02), 649 (0.01)	650	1.8 ± 0.2	8.7 ± 0.2
DAEPor	417 (1.5), 514 (0.07), 549 (0.03), 586 (0.02), 648 (0.01)	652	1.6 ± 0.1	6.5 ± 0.1
DABPor	417 (1.4), 513 (0.7), 549 (0.03), 587 (0.02), 645 (0.01)	651	1.9 ± 0.1	7.2 ± 0.1
DAHPor	417 (1.8), 513 (0.08), 548 (0.03), 589 (0.02), 645 (0.01)	651	1.8 ± 0.2	7.1 ± 0.1

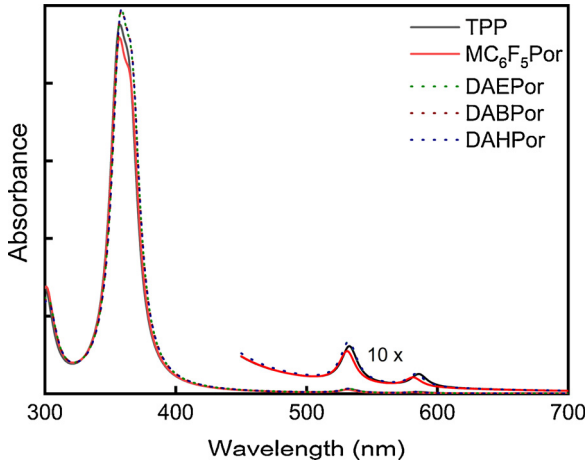

Fig. 3. Theoretical absorption spectra by TD-DFT for the studied porphyrins, using DCM as solvent.

this molecule, ferrocene moiety is closer to the porphyrinic ring, increasing the electrostatic interaction. The fluorescence lifetimes, also shown in Table 1 and obtained with time resolved fluorescence technique, are in agreement with the values found in the literature for free-base porphyrins 42 and ferrocenyl-porphyrins [43].

It is interesting to point out that the optical properties described until this point are in accordance to the ones observed in the theoretical analysis. As it will be described in the next section, the linear absorptions of all compounds are very similar, with no significant changes due to the ferrocene moiety. Also, the charge distributions on the natural transition orbitals are comparable.

3.2. Theoretical (TD-DFT) analysis

In Fig. 3 and Table 2, we show the theoretical (TD-DFT) optical absorption data for all the free-based porphyrins studied in this work. These data were obtained at the ground state equilibrium geometry of each considered molecule. As a general feature, one peak is observed for the Soret band (˜355 nm), and other peaks representing the Q-bands at *c.a.* 530 nm and *c.a.* 580 nm, for all molecules. All compounds share very similar optical absorption behavior, with no significant effect related to the introduction (or the size) of the aliphatic chains connecting the ferrocene to the macrocycle.

In order to better understand the optical transitions predicted by the TD-DFT calculations, in Fig. 4 we show the natural transition orbitals (NTOs) associated with both Soret and Q-band transitions of Fig. 3. From Fig. 4, we can observe that these natural transition orbitals are very similar for all tetrapyrrolic macrocycles. The orbitals involved in the electronic absorption transitions, named HOMO and LUMO here, are localized on the porphyrin ring. The charge distribution patterns of these orbitals are very similar for both Soret and Q-bands, independently of the considered compound. From these results one can state that the length of the aliphatic chain bounding the C_6F_4 to the ferrocene do not significantly influence the electronic transitions related to the absorption spectra.

Table 2
Calculated energies (E), wavelengths (λ) oscillator strengths (f) for the NTOs of the studied porphyrins.

Porphyrin	λ (nm)	E (eV)	Oscilator strength (f)
TPP	356	3.483	1.66
	533	2.326	0.03
MC_6F_5Por	355	3.493	1.65
	531	2.335	0.02
DAEPor	356	3.483	1.77
	532	2.331	0.03
DABPor	357	3.473	1.75
	532	2.331	0.03
DAHPor	357	3.473	1.75
	532	2.331	0.03

3.3. Nonlinear optical experiments

Excited state characterization of all (amino-ferrocenyl)porphyrins studied in this work were obtained for the first time by employing a set of techniques involving nonlinear optical spectroscopy. Here, several techniques were used for the determination of the optical parameters related to the excited singlet and triplet states. Firstly, the Z-Scan by single pulse technique was used to determine the first excited singlet state absorption cross-section at 532 nm (σ_{1n}(λ= 532 nm)). It is important to note that the absorption cross section at this wavelength will serve as the verification parameter of the absorption cross-section spectra ($\sigma_{1n}(\lambda)$) in the UV–vis region, obtained through the Z-scan by white light technique. As already mentioned, Z-Scan by single pulse is based on monitoring the normalized transmittance (NT) of a material as it is translated around a previously focused pulsed laser beam. Due to the focus of the laser beam (which gives a profile of different intensities for each Z position of the translation region), when the sample is far from the focal point, only linear effects are felt by the material, however, as the sample approaches the focus, there is a gradual increase in intensity, thus the nonlinear effects become more pronounced. However, in order to obtain the normalized transmittance, NT, the transmittance is first measured away from the focus and then, transmittances are obtained for each Z position getting to the focus point. Finally, the transmittances obtained for each Z point are divided by the transmittance obtained away from the focus.

The determination of the σ_{1n}(λ= 532 nm) is accomplished through the theoretical modeling of NT obtained experimentally. This is performed through population dynamics modeling of a system using three singlet energy levels (S) and two triplet energy levels (T). After energy absorption, the electrons of the material are promoted from the fundamental singlet state (S_0) to a singlet excited state (S_1), however, if the material continues to absorb energy, such electrons can populate higher energy levels. By modeling such population dynamics through the Beer-Lambert law and the rate equations, it is possible to obtain a theoretical normalized transmittance.

It is important to mention here that for the Z-Scan by single pulse, we could neglect the two triplet energy levels (T_1 and T_n), because the pulse width (100 ps) is shorter than the porphyrin's intersystem crossing time (ns), in a way that there is not enough time to populate the triplet energy levels. The rate equations for the three energy levels which describe the population fraction in the energy levels n_S ´s, schematic represented in Fig. 5, are:

$$\begin{aligned} \frac{dn_{S_0}(t)}{dt} &= -W_{01}^S n_{S_0}(t) + K_{10}^S n_{S_1}(t) \\ \frac{dn_{S_1}(t)}{dt} &= W_{01}^S n_{S_0}(t) - K_{10}^S n_{S_1}(t) - W_{1n}^S n_{S_1}(t) + K_{n1}^S n_{S_n}(t) \\ \frac{dn_{S_n}(t)}{dt} &= W_{1n}^S n_{S_1}(t) - K_{n1}^S n_{S_n}(t) \end{aligned} \quad (2)$$

in which, $K_{n1} = 1/\tau_{n1}$ and $K_{10} = 1/\tau_{10}$ are the decay rates, respectively, from the electronic state 1 to 0 and from n to 1. $W_{m;m+1} = \frac{I(t)\sigma_{m;m+1}}{h\nu}$ is defined as transition probability from a lower energetic state (m) to a higher one ($m + 1$), in which $I(t)$ is the laser intensity, $\sigma_{m;m+1}$ is the absorption cross section from an electronic state m to an electronic state m + 1, in which m can be 0, 1 or n. h is the Planck constant, and ν is the frequency of light. $n_{s_0} + n_{s_1} + n_{s_n} = 1$ is the boundary condition. In this case, K_{10} can be considered low because the pulse laser is much shorter than the fluorescence lifetime. Normally, for free based porphyrins, τ_{n1} is of about 300 fs which gives a high K_{n1}. This high decay rate describes a non-cumulative population at state S_n. Consequently, the absorption

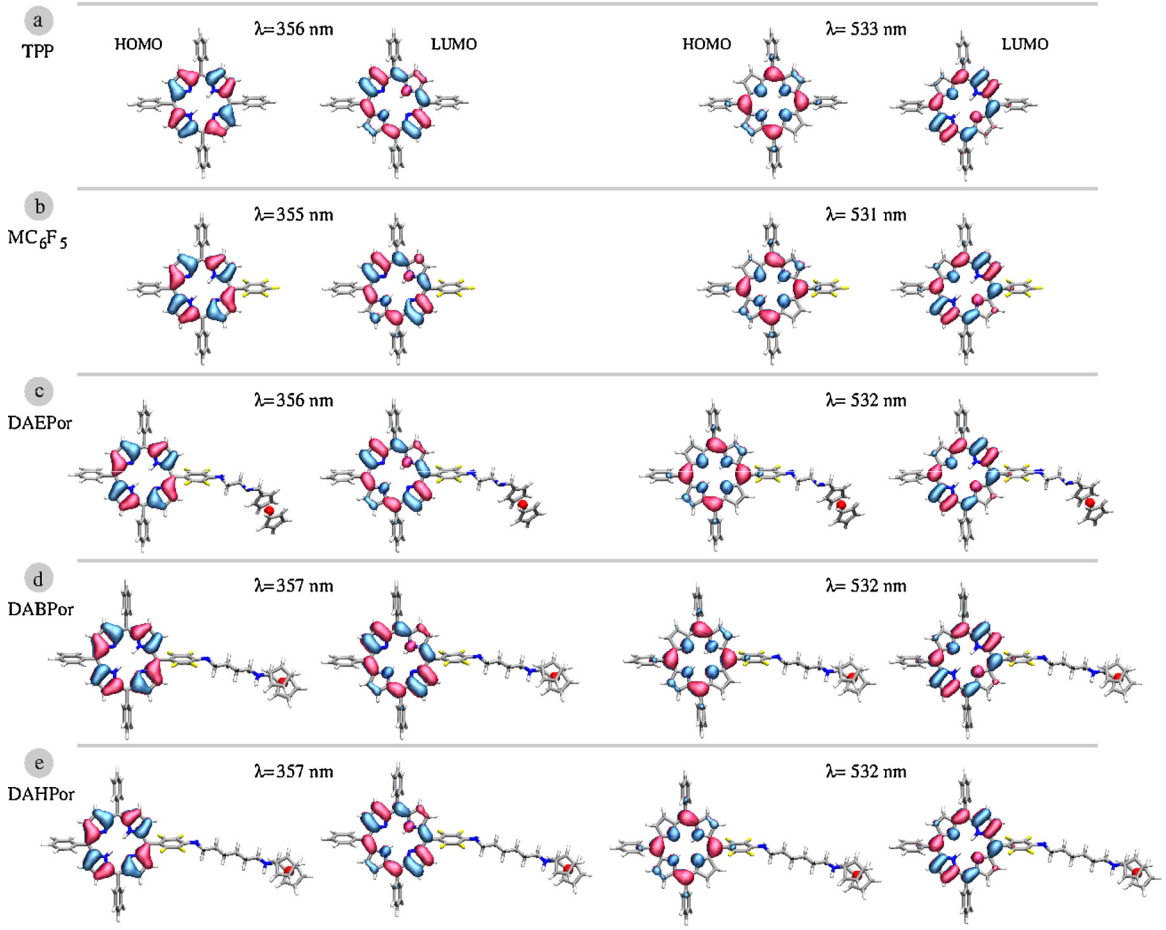

Fig. 4. Natural transition orbitals associated with the absorption peaks presented in Fig. 3.

coefficient, $\alpha(t)$ can be obtained by $\alpha(t, 532\,nm) = N[n_{S_0}(t)\sigma_{01}(532\,nm) + n_{S_1}(t)\sigma_{1n}(532\,nm)]$ with N the concentration in molelules/cm^3 of the samples.

The numerical solution of these rate equations was carried out by a homemade program that takes into account the parameters previously determined by linear optical spectroscopy. In this way, the theoretical fitting of the experimental normalized transmittance was performed by adjusting the singlet excited state absorption cross section $\sigma_{1n}(532\,nm)$. These adjustments (solid lines) are shown in Fig. 5 for the **MC_6F_5Por** and **DAHPor** molecules.

Fig. 5 shows the Z-Scan for two of the five substituted-ferrocenyl porphyrin molecules. It is important to say that all molecules have the same Z-Scan by single pulse profile. In Fig. 5, it is clear that as the intensity of the laser beam increases or, in other words, as the sample approaches the focal point, NT decreases until it reaches a minimum at Z = 0, indicating that the material is absorbing more energy since there is an increase in intensity. Hence, the first excited singlet state cross-section is larger than the ground singlet absorption cross-section

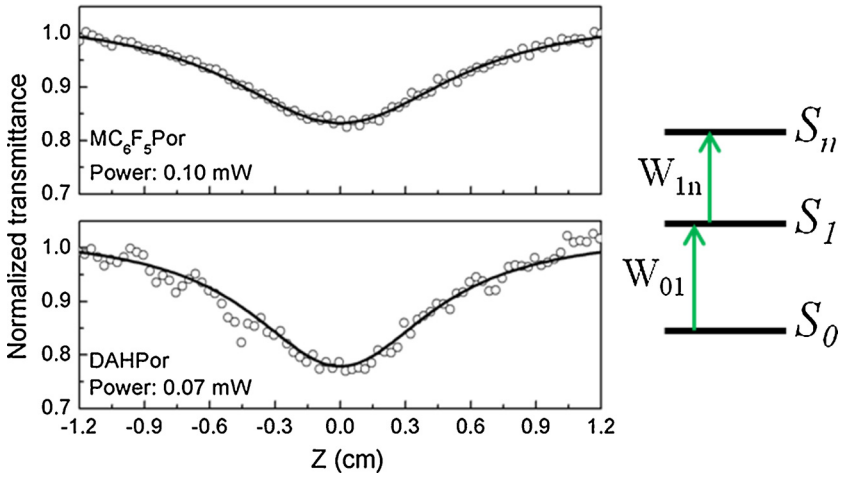

Fig. 5. Experimental normalized transmittance obtained by Z-Scan by single pulse (black circles) and theoretical normalized transmittance (black line) obtained through the numerical solution of the rate equations for three energy levels as depicted.

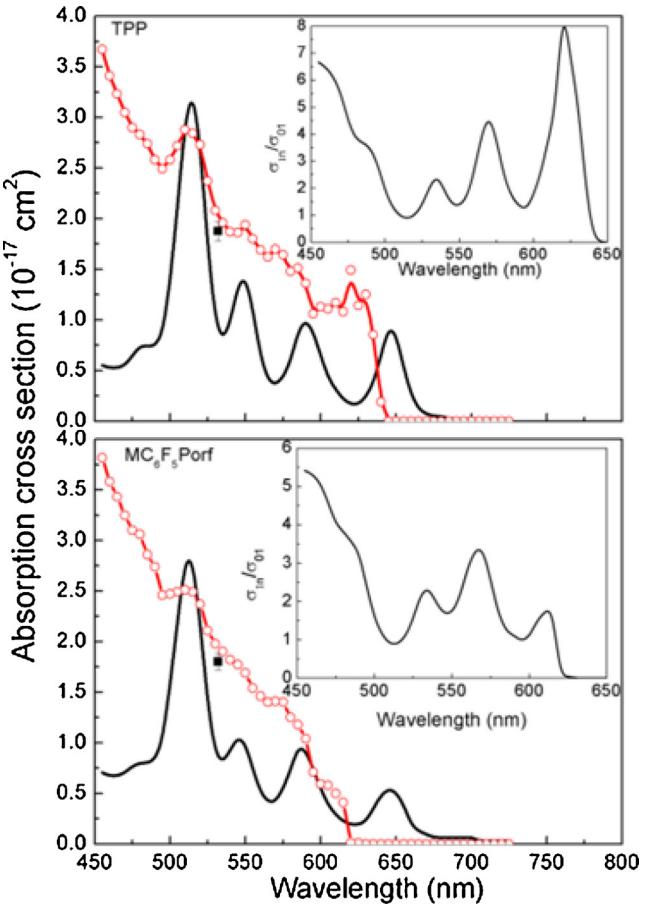

Fig. 6. Ground (black line) and excited (open red circles) absorption cross sections spectra for **TPP** and **MC$_6$F$_5$Por** dissolved in DCM. Black square represents absorption cross section at 532 nm determined by Z-Scan by single pulse. The inset in each graph shows the ratio between the excited state absorption cross-section and ground state.

($\sigma_{1n} > \sigma_{01}$).

The values of the excited singlet state absorption cross section at 532 nm, obtained through the adjustment between the theoretical and experimental NT, are very similar for all studied molecules (approximately $1.7 \pm 0.2 \times 10^{-17}$ cm^2), showing that the absorption cross-sections of the first excited state are not significantly altered by the differences in the chemical structures of the molecules, which also agrees with the linear spectroscopic data and theoretical calculations. The values (black squares) are shown in Figs. 6 and 7 and compared to the ones obtained with white-light continuum Z-Scan. The order of magnitude of the excited state absorption cross-section is also in agreement with ones reported for free-base pophyrins [44–48].

White light continuum Z-Scan was used for the determination of the excited state absorption cross-section in a range from about 450–700 nm. This technique is also based on Z-Scan by single pulse by monitoring the NT while the material is translated around a previously focused beam. However, in the Z-Scan via white light, the pulse is a supercontinuum broadband light that ranges approximately from 450 to 700 nm. For each wavelength of that supercontinuum, a Z-Scan, similarly to the single pulse Z-Scan, is acquired, and the absorption cross sections of the excited singlet state, as a function of the wavelength, are determined. The normalized transmittance is monitored for each Z position and for each wavelength that makes up the supercontinuum. In the same way as in Z-Scan by single pulse, it is possible to simulate the population dynamics considering three energy levels described in Eq. (2) and, consequently, to theoretically obtain NT. However, $\alpha(t, \lambda) = N[n_{S_0}(t)\sigma_{01}(\lambda) + n_{S_1}(t)\sigma_{1n}(\lambda)]$ is now wavelength dependent.

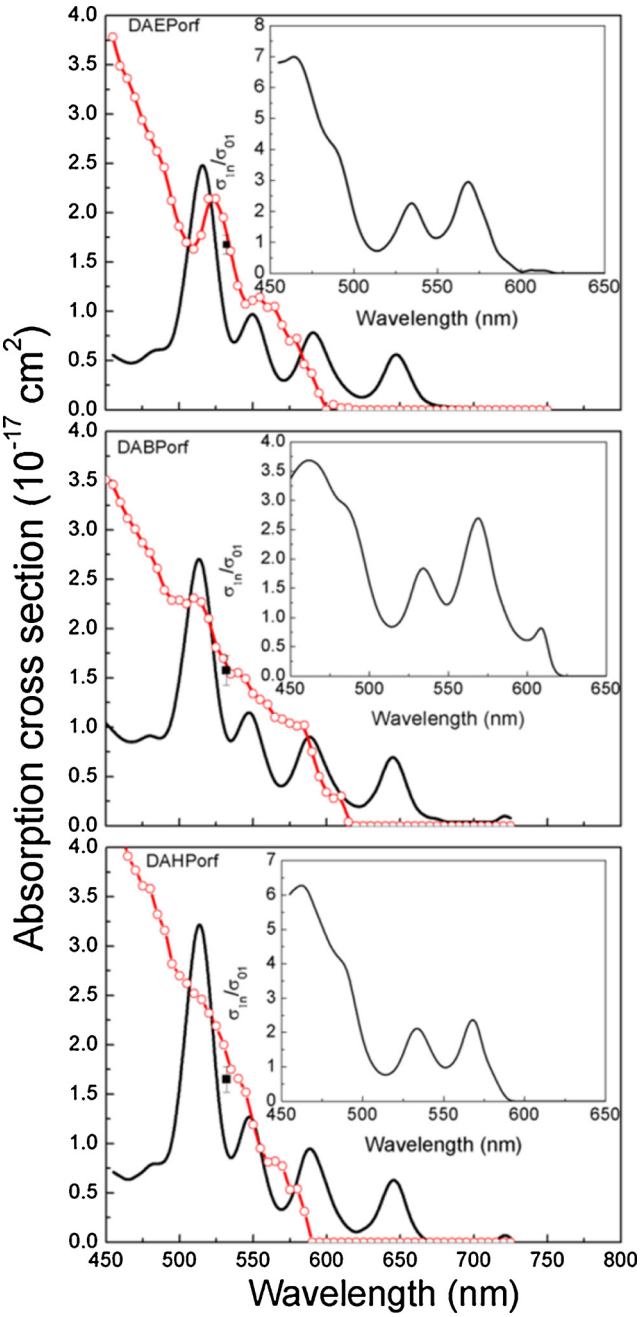

Fig. 7. Absorption cross-sections of studied porphyrins dissolved in DMSO. Ground state (black line), first excited state (open red circles). Excited state absorption cross section at 532 nm determined by Z-Scan by single pulse (black square). The ratio between the excited state absorption cross-section and ground state are depicted at the figure insets.

Through Figs. 6 and 7, we can see similarities between the excited states absorption cross section of the five porphyrins (open red circles), indicating that the distinct peripheral structures do not change significantly the excited state absorption cross section. In addition, the good agreement between the single pulse Z-Scan technique (see black square in Figs. 6 and 7) and the white light Z-Scan confirms that at ˜530 nm the excited state absorption cross section is higher than the ground state one.

Fig. 6 displays the excited state absorption cross-section for **TPP** and **MC$_6$F$_5$Por**, both without ferrocene moieties. It is possible to see, by comparing both molecules, that the excited state absorption cross sections all along the spectrum present almost the same values, as

considering the experimental error of about 10%. This statement is in agreement to the one observed for the ground state absorption, and also to the molecular orbitals associated with the electronic transitions, which are similar for both molecules.

The excited state absorption cross sections show a monotonic increase of their values for shorter wavelengths. Important information that reveals the absorption strength of the excited state is also given by the ratio between the excited and ground state absorption cross-sections, which can be seen in the insets of Fig. 6. For most wavelengths, the ratio is higher than the unit, which reveals that the molecules increase the absorption efficiency at the excited state and can be used as optical limiters at the visible region. For some wavelengths, the ratio value achieves a factor of about five times, indicating a strong absorption in the molecular excited singlet state.

Fig. 7 exhibits the excited state absorption cross sections of the three amino-ferrocenyl porphyrins dissolved in DMSO solvent. The excited state absorption cross sections all along the spectrum are of the same order of magnitude, comparing all three molecules, and are also very similar to **TPP** and **MC$_6$F$_5$Por**. Similar spectral characteristics were noticed in these three molecules, where a monotonic increase of the excited state absorption cross sections for shorter wavelengths is observed. Excited state absorption has been reported in many different free based porphyrins, indicating an increase in the absorption at the visible region [49–52].

Following the same features of **TPP** and **MC$_6$F$_5$Por**, ferrocene porphyrins present a ratio between the absorption cross sections higher than the unit for most of the wavelengths and may also be used as optical limiters. It is important to mention here that the length of the aliphatic chain, binding **C$_6$F$_4$** to the ferrocene, seems to restrict significantly the influence of ferrocene to the porphyrin, preserving the ground and the excited state absorption cross section at the same magnitude as the ones evaluated for **TPP** and **MC$_6$F$_5$Por**. An important information about the excited state optical properties for these set of molecules is the weak influenced of the presence of the ferrocene moiety, as shown by the ground state absorption and TD-DFT theoretical calculations.

Once the parameters for the singlet excited state absorption have been determined, we set out to determine the triplet state electronic parameters. The triplet excited state absorption cross section and the intersystem crossing time from the first singlet excited state to the triplet state were evaluated for all five porphyrins studied in this work. It was determined by monitoring changes in the absorption, similarly to the ones measured by Z-Scan with single pulse and white light supercontinuum. However, in this case, as the singlet electronic absorption was already determined previously by single pulses techniques, the normalized transmittance (NT) induced by the pulse train brings information of the population transferred to the triplet state. NT obtained from this technique is now numerically simulated by using the five energy levels diagram, as schematically represented in Fig. 8. The best fit obtained, which was determined considering all singlet parameters determined previously, gives the absorption cross section of the triplet state and the intersystem crossing time. To simulate the population fraction transferred from the ground state (S_0) to excited singlet states n_S ´s and triplet state n_T ´s, five rate equations were solved numerically:

$$\frac{dn_{S0}(t)}{dt} = K_{ic}^{S} n_{S1}(t) + K_{r}^{S} n_{S1}(t) - W_{01}^{S} n_{S0}(t)$$

$$\frac{dn_{S1}(t)}{dt} = W_{01}^{S} n_{S0}(t) + K_{n1}^{S} n_{Sn}(t) - (K_{r}^{S} + K_{ic}^{S} + K_{isc}) n_{S1}(t) - W_{1n}^{S} n_{S1}(t)$$

$$\frac{dn_{Sn}(t)}{dt} = W_{1n}^{S} n_{S1}(t) - K_{1n}^{S} n_{Sn}(t) \qquad (3)$$

$$\frac{dn_{T1}(t)}{dt} = K_{isc} n_{S1}(t) + K_{n1}^{T} n_{Tn}(t) - W_{1n}^{T} n_{T1}(t)$$

$$\frac{dn_{Tn}(t)}{dt} = W_{1n}^{T} n_{T1}(t) - K_{n1}^{T} n_{Tn}(t)$$

in which, $K_{n1}^{S} = 1/\tau_{n1}$ and $K_{n1}^{T} = 1/\tau_{n1}$ are the decay rates, respectively, from the electronic n to 1 from the singlet (S) and triplet (T) states. For both, τ_{n1} is of about 300 fs which gives a high K_{n1}. . $W_{nm}^{S\,or\,T} = \frac{I(t)\sigma_{m=m+1}}{h\nu}$ is defined as the transition probability from a lower energetic state (m) to a higher one ($m + 1$) in the singlet-singlet transition (S) or triplet-triplet (T) transition. $I(t)$ is the laser intensity, $\sigma_{m;m+1}$ is the absorption cross section from an electronic state m to an electronic state m + 1, in which m can be 0, 1 or n. h is the Planck constant, and ν is the frequency of light. $n_{s_0} + n_{s_1} + n_{s_n} = 1$ is the boundary condition. K_r is the radiative rate, K_{ic} is the internal conversion rate and K_{isc} is the intersystem crossing rate. Normally, for free based porphyrins. This high decay rate describes a non-cumulative population at state S_n.

In this case, the dynamical absorption coefficient considering also the triplet states is described as $\alpha(t, \lambda) = N[n_{S0}(t)\sigma_{01}(532nm) + n_{S1}(t)\sigma_{1n}(532nm) + n_{T1}(t)\sigma_{t}(532nm)]$. In Fig. 8, the solid lines represent the adjustments of the experimental NT's, as a function of the pulse number of the pulse train, obtained by solving the Eq. (3).

Values of the triplet state absorption cross sections obtained through the adjustments are: (1.8 ± 0.4) x 10^{-17} cm^2 for **TPP**, (2.1 ± 0.3) x 10^{-17} cm^2 for **MC$_6$F$_5$Por**, (2.0 ± 0.2) x 10^{-17} cm^2 for **DAEPor**, (1.7 ± 0.2) x 10^{-17} cm^2 for **DABPor** and (1.9 ± 0.2) x 10^{-17} cm^2 for **DAHPor**. We noted that, considering the experimental error, all values are approximately the same, indicating that peripheral structures do not significantly change the absorption strength of the molecules in the triplet state for a wavelength of about 532 nm. On the other hand, the values for the intersystem crossing time were slightly influenced by the presence of C_6F_4 and ferrocene moiety. From **TPP** dissolved in DCM, it was found an intersystem crossing time of about 21.0 ± 0.6 ns. When C_6F_4 group is added at the porphyrin *meso* position, a reduction in the intersystem crossing time of about 7% was observed for **MC$_6$F$_5$Por** (19.5 ± 0.5) ns. Since the fluorescence lifetime for both porphyrins can be considered identical (see Table 1) but the fluorescence quantum yield is less intense in **MC$_6$F$_5$Por**, nonradiative processes such as internal conversion or intersystem crossing time should increase their efficiency. For the case of the three ferrocene porphyrins, intersystem crossing times were obtained and considered indistinguishable within the experimental error of the technique: (17.0 ± 1.0) ns for **DAEPor**, (17.5 ± 0.5) ns for **DABPor** and (16.5 ± 0.5) ns for **DAHPor**. However, all values were lower than for **TPP** and **MC$_6$F$_5$Por** of about 19% and 13% respectively. Based on these values, we can also conclude that the length of the aliphatic chain is not affecting significantly the intersystem crossing time of these three molecules.

Finally, for better visualization and understanding of the results obtained by photophysical studies made in this work, we also determined the radiative and internal conversion rates, as shown in Table 3. Intersystem crossing decay rate was calculated directly from the intersystem crossing time by using $k_{isc} = 1/\tau_{isc}$., and, as can be seen in Table 3, the highest rates were obtained for the ferrocene porphyrins. The radiative decay rate was obtained by the ratio between the fluorescence quantum yield and fluorescence lifetime as $k_r = \phi_f/\tau_f$. The lowest radiative rate was observed for **MC$_6$F$_5$Por**; however, the values do not differ significantly from each other.

Internal conversion rate, that indicates nonradiative process from the first singlet excited state to the ground state was obtained by $k_{ic} = k_f - k_r - k_{isc}$, in which $k_f = 1/\tau_f$. Calculated values reveal that this process is more efficient for **DAEPor** molecule, followed by **DABPor**, which is in agreement with the shortest fluorescence lifetime. The proximity of the ferrocene unit to the **C$_6$F$_4$** in **DAEPor** increases the nonradiative rate and quenches the fluorescence due to the higher interaction between the iron ion and the porphyrin ring. This is in accordance to what was described for ferrocenes units in BODIP molecules [42]. As the length of the aliphatic chain increases, nonradiative

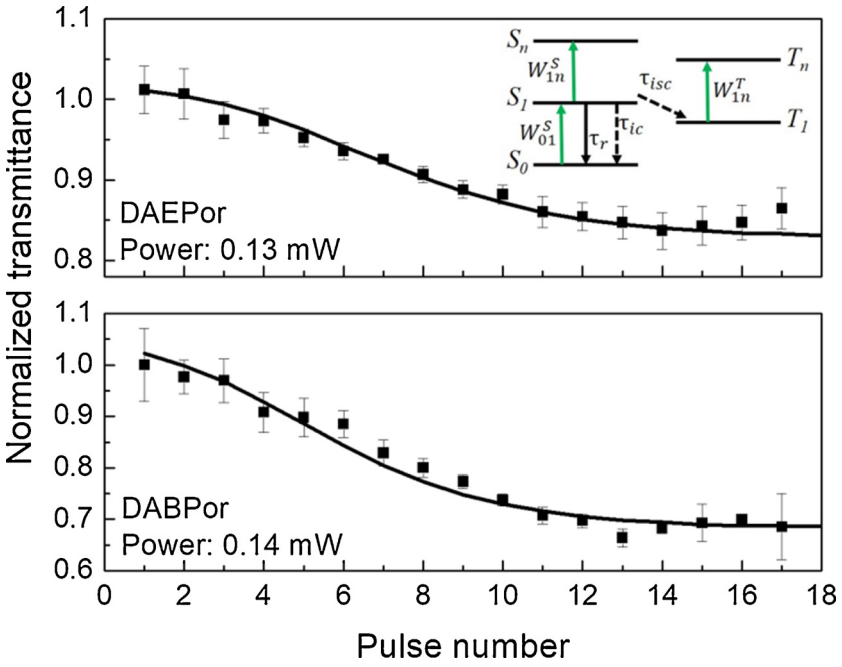

Fig. 8. Experimental normalized transmittance (NT) for each pulse of the pulse train (black squares) and theoretical normalized transmittance (black line) obtained through the solution of the rate equations for five energy levels diagram as depicted.

Table 3
Fluorescence lifetime, radiative, internal conversion and intersystem crossing rates constants for porphyrins dissolved in DCM.

Porphyrin	τ_f (ns)	$k_r(10^6 s^{-1})$	$k_{ic}(10^6 s^{-1})$	$k_{ISC}(10^6 s^{-1})$
TPP	8.7	2.8	65	47
MC_6F_5Por	8.5	2.2	64	51
DAEPor	6.4	2.5	95	59
DABPor	7.2	2.6	79	57
DAHPor	7.1	2.5	77	61

rate decreases its value to the ones close to **TPP** and **MC_6F_5Por**. The fact that the ferrocene unit is separated by a non-conjugated spacer, and, consequently, the charge interaction is not so effective, explains why the optical properties of the porphyrins are only slightly affected in these molecular systems.

The triplet state formation was determined by using $\phi_T = \tau_f/\tau_{isc}$. It was observed that **MC_6F_5Por** and **DAHPor** presented the best triplet formation of the five porphyrins, followed by **TPP** and **DABPor**. The results are presented in Fig. 9, together with fluorescence and internal conversion quantum yields. The lowest triplet quantum yield of about 37.6% was obtained for **DAEPor**. As can be seen, the intersystem crossing rate for **DAEPor** is not the lowest one (see Table 3); nevertheless, its internal conversion rate is the highest, which explains a decrease in the triplet quantum yield. Looking at Fig. 9, we observe that internal conversion process (green bars), obtained by $\phi_T = 1 - \phi_f - \phi_T$, is the most favorable mechanism for the deactivation of first excited state for all five porphyrins, with values close to 55%.

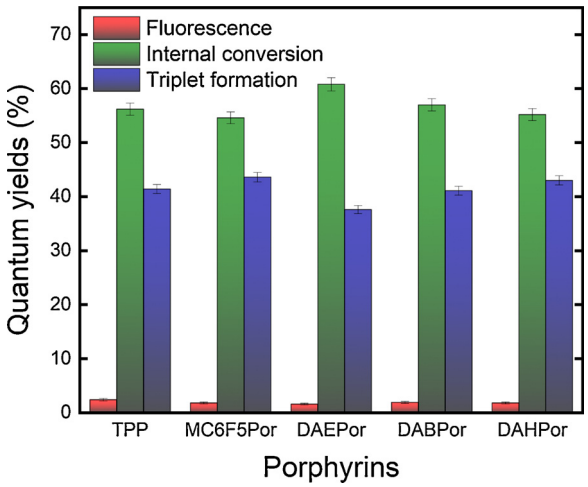

Fig. 9. Fluorescence, internal conversion and triplet formation quantum yields, expressed in % for the five porphyrins studied in this work, all dissolved in DCM solvent.

4. Conclusion

In summary, amino-ferrocene moieties attached to the **TPP** porphyrin show to slightly modify some photophysical properties of the main porphyrinic ring. One can see that the absorption cross-sections of the ground and first excited states, followed by absorption of the triplet state at 532 nm, are not considerably modified from **TPP** to **MC_6F_5Por**, as well as for the three amino-ferrocenyl porphyrins, within the experimental error. However, the rates involved in the deactivation processes of the first excited state are the ones that suffer some changes due to the molecular structure modification. Fluorescence quantum yield is affected when the ferrocenyl moiety with the shortest aliphatic chain is binding to the **MC_6F_5Por**, increasing the internal conversion process. However, as the aliphatic chain length increases, the photophysical processes tend to be numerically close to the ones obtained for **TPP** and **MC_6F_5Por**. The lowest triplet quantum yield formation was evaluated for **DAEPor**, which indicates that the internal conversion process is the main mechanism for these molecules.

Based on the photophysical experiments supported by the TD-DFT calculations of the studied molecules, it was possible to prove that these characteristics are independent of the size of the spacer connected in the *meso*-aryl position of the porphyrin. Future works and investigations will be conducted in order to improve the understanding of effects such as changing from aliphatic to aromatic or conjugated spacers, and also the insertion of other substituents at the periphery of porphyrin to control their photophysical properties, since these derivatives have a

great interest for interactions with biomolecules (DNA and proteins) as well as in bio-electrochemical sensors (using the ferrocene unit as a probe).

Acknowledgements

This study was financed in part by the Coordenação de Aperfeiçoamento de Pessoal de Nível Superior – Brasil (CAPES) – Finance Code 001 and FAPESP by funding researchers. Bernardo A. Iglesias (Universal Grants 409150/2018-5, PQ Grants 304711/2018-7 and Finance Code 001), Paulo C. Piquini (Grants 312388/2018-7), and Leonardo de Boni (Grants 404541/2016-0) thanks the Conselho Nacional de Desenvolvimento Científico e Tecnológico also thanks Fundação de Amparo à Pesquisa do Estado de São Paulo (FAPESP – Brazil; Grants 2016/20886-1).

Appendix A. Supplementary data

Supplementary material related to this article can be found, in the online version, at doi:https://doi.org/10.1016/j.jphotochem.2019.112048.

References

[1] J. Uddin, Macro to Nano Spectroscopy, InTechOpen, London, United Kingdom, 2012, p. 448.
[2] L.H.Z. Cocca, M.M. Ayhan, A.G. Gürek, V. Ahsen, Y. Bretonniére, J.P. Siqueira, F. Gotardo, C.R. Mendonça, C. Hirel, L. De Boni, Mechanism of the Zn(II) Phthalocyanines' photochemical reactions depending on the number of substituents and geometry, Molecules 21 (2016) 635.
[3] G. de la Torre, P. Vázquez, F. Agulló-López, T. Torres, Role of structural factors in the nonlinear optical properties of Phthalocyanines and related compounds, Chem. Rev. 104 (2004) 3723–3750.
[4] M.O. Senge, M. Fazekas, E.G.A. Notaras, W.J. Blau, M. Zawadzka, O.B. Locos, E.M. Ni Mhuircheartaigh, Nonlinear optical properties of porphyrins, Adv. Mater. 19 (2007) 2737–2774.
[5] M.J. Stillman, T. Nyokong, C.C. Leznoff, A.B.P. Lever, Phthalocyanines: Properties and Applications, VCH, New York, 1989.
[6] K.M. Kadish, K.M. Smith, R. Guilard, The Porphyrin Handbook vol. 1–20, Academic Press, San Diego, 2000.
[7] M. Calvete, G.Y. Yang, M. Hanack, Porphyrins and phthalocyanines as materials for optical limiting, Synth. Met. 141 (2004) 231–243.
[8] P. Gautam, B. Dhokale, V. Shukla, C.P. Singh, K.S. Bindra, R. Misra, Optical limiting performance of *meso*-tetraferrocenyl porphyrin and its metal derivatives, J. Photochem. Photobiol. A: Chem. 239 (2012) 24–27.
[9] A. Krivokapic, H.L. Anderson, G. Bourhill, R. Ives, S. Clark, K.J. McEwan, *Meso*-Treta-Alkynyl porphyrins for optical limiting – a survey of group III and IV metal complexes, Adv. Mater. 13 (2001) 652–656.
[10] D. Dini, M.J.F. Calvete, M. Hanack, Nonlinear optical materials for the smart filtering of optical radiation, Chem. Rev. 116 (2016) 13043–13233.
[11] E.G.A. Notaras, M. Fazekas, J.J. Doyle, W.J. Blau, M.O. Senge, A_2B_2-type push–-pullporphyrins as reverse saturable and saturable absorbers, Chem. Commun. (2007) 2166–2168.
[12] H. Wang, L. Xiao, L. Yan, S. Chen, X. Zhu, X. Peng, X. Wang, W.-K. Wong, W.-Y. Wong, Structural engineering of porphyrin-based small molecules as donors for efficient organic solar cells, Chem. Sci. 7 (2016) 4301–4307.
[13] K. Gao, L. Li, T. Lai, L. Xiao, Y. Huang, F. Huang, J. Peng, Y. Cao, F. Liu, T.P. Russell, R.A.J. Janssen, X. Peng, Deep absorbing porphyrin small molecule for high-performance organic solar cells with very low energy losses, J. Am. Chem. Soc. 137 (2015) 7282–7285.
[14] J. Kou, D. Dou, L. Yang, Porphyrin photosensitizers in photodynamic therapy and its applications, Oncotarget 8 (2017) 81591–81603.
[15] X. Wang, P. Wang, S. Xue, X. Zheng, Z. Xie, G. Chen, T. Sun, Nanoparticles based on glycyrrhetinic acid modified porphyrin for photodynamic therapy of cancer, Org. Biomol. Chem. 16 (2018) 1591–1597.
[16] F. Bolze, S. Jenni, A. Sour, V. Heitz, Molecular photosensitisers for two-photon photodynamic therapy, Chem. Commun 53 (2017) 12857–12877.
[17] N.B. Thornton, H. Wojtowicz, T. Netzel, D.W. Dixon, Intramolecular quenching of porphyrin fluorescence by a covalently linked ferrocene in DNA scaffolding, J. Phys. Chem. B 102 (1998) 2101–2110.
[18] B.L. Auras, S.L. Meller, M.P. Silva, A. Neves, L.H.Z. Cocca, L. De Boni, C.H. da Silveira, B.A. Iglesias, Synthesis, spectroscopic/electrochemical characterization and DNA interaction study of novel ferrocenyl-substituted porphyrins, Appl. Organometal. Chem 32 (2018) e4318.
[19] G. Pratviel, Porphyrins in complex with DNA: modes of interaction and oxidation reactions, Coord. Chem. Rev. 308 (2016) 460–477.
[20] L.M.O. Lourenço, B.A. Iglesias, P.M.R. Pereira, H. Girão, R. Fernandes, M.G.P.M.S. Neves, J.A.S. Cavaleiro, J.P.C. Tomé, Synthesis, characterization and biomolecule-binding properties of novel tetra-platinum(II)-thiopyridylporphyrins, Dalton Trans. 44 (2015) 530–538.
[21] B.L. Auras, V.A. Oliveira, H. Terenzi, A. Neves, B.A. Iglesias, Meso-Mono-[4-(1,4,7-triazacyclononanyl)]-tri(phenyl)]porphyrin and the respective zinc(II)-complex: complete characterization and biomolecules binding abilities, Photochem. Photobiol. Sci. 15 (2016) 564–579.
[22] V.A. Oliveira, B.A. Iglesias, B.L. Auras, A. Neves, H. Terenzi, Photoactive meso-tetra (4-pyridyl)porphyrin-tetrakis-[chloro(2,2′bipyridine)platinum(II) derivatives recognize and cleave DNA upon irradiation, Dalton Trans. 46 (2017) 1660–1669.
[23] M.J.F. Calvete, S.M. Pinto, Synthesis of Pyrrole-Based Macrocycles as molecular probes for multimodal imaging techniques: recent trends, Curr. Org. Synth. 14 (2017) 704–714.
[24] C. Moylan, E.M. Scanlan, M.O. Senge, Chemical synthesis and medicinal applications of glycoporphyrins, Curr. Med. Chem. 22 (2015) 2238–2348.
[25] N.V.S.D.K. Bhupathiraju, W. Rizvi, J.D. Batteas, C.M. Drain, Fluorinated porphyrinoids as efficient platforms for new photonic materials, sensors, and therapeutics, Org. Biomol. Chem. 14 (2016) 389–408.
[26] L. Lvova, P. Galloni, B. Floris, I. Lundström, R. Paolesse, C. Di Natale, A ferrocene-porphyrin ligand for multi-transduction chemical sensor development, Sensors 13 (2013) 5841–5856.
[27] A. Vecchi, E. Gatto, B. Floris, V. Conte, M. Venanzi, V.N. Nemykin, P. Galloni, Tetraferrocenylporphyrins as active components of self-assembled monolayers on gold surface, Chem. Commun 48 (2012) 5145–5147.
[28] L.M.O. Lourenço, J. Resende, B.A. Iglesias, K. Castro, S. Nakagaki, M.J. Lima, A.F. da Cunha, M.G.P.M.S. Neves, J.A.S. Cavaleiro, J.P.C. Tomé, Synthesis, characterization and electrochemical properties of meso-thiocarboxylate-substituted porphyrin derivatives, J. Porphyr. Phthalocyan 18 (2014) 967–974.
[29] M.J. Frisch, G.W. Trucks, H.B. Schlegel, G.E. Scuseria, M.A. Robb, J.R. Cheeseman, G. Scalmani, V. Barone, B. Mennucci, G.A. Petersson, H. Nakatsuji, M. Caricato, X. Li, H.P. Hratchian, A.F. Izmaylov, J. Bloino, G. Zheng, J.L. Sonnenberg, M. Hada, M. Ehara, K. Toyota, R. Fukuda, J. Hasegawa, M. Ishida, T. Nakajima, Y. Honda, O. Kitao, H. Nakai, T. Vreven, J.A. Montgomery Jr., J.E. Peralta, F. Ogliaro, M. Bearpark, J.J. Heyd, E. Brothers, K.N. Kudin, V.N. Staroverov, R. Kobayashi, J. Normand, K. Raghavachari, A. Rendell, J.C. Burant, S.S. Iyengar, J. Tomasi, M. Cossi, N. Rega, J.M. Millam, M. Klene, J.E. Knox, J.B. Cross, V. Bakken, C. Adamo, J. Jaramillo, R. Gomperts, R.E. Stratmann, O. Yazyev, A.J. Austin, R. Cammi, C. Pomelli, J.W. Ochterski, R.L. Martin, K. Morokuma, V.G. Zakrzewski, G.A. Voth, P. Salvador, J.J. Dannenberg, S. Dapprich, A.D. Daniels, Farkas, J.B. Foresman, J.V. Ortiz, J. Cioslowski, D.J. Fox, Gaussian 09, Revision C, Gaussian, Inc., Wallingford CT, 2009.
[30] T. Yanai, D.P. Tew, N.C. Handy, A new hybrid exchange–correlation functional using the Coulomb-attenuating method (CAM-B3LYP), Chem. Phys. Lett. 393 (2004) 51–57.
[31] W.J. Hehre, R. Ditchfield, J.A. Pople, Self—consistent molecular orbital methods. XII. Further extensions of Gaussian—type basis sets for use in molecular orbital studies of organic molecules, J. Chem. Phys. 56 (1972) 2257–2261.
[32] A.C. Bevilacqua, M.H. Köhler, B.A. Iglesias, P.C. Piquini, Photophysical and photocatalytic properties of corrophyll and chlorophyll, Comput. Mat. Sci 158 (2019) 228–234.
[33] J. Tomasi, B. Mennucci, R. Cammi, Quantum mechanical continuum solvation models, Chem. Rev. 105 (2005) 2999–3094.
[34] R.C. Pivetta, B.L. Auras, B. de Souza, A. Neves, F.S. Nunes, L.H.Z. Cocca, L. De Boni, B.A. Iglesias, Synthesis, photophysical properties and spectroelectrochemical characterization of 10-(4-methyl-bipyridyl)-5,15-(pentafluorophenyl)corrole, J. Photochem. Photobiol. A: Chem. 332 (2017) 306–315.
[35] L. De Boni, C. Toro, F.E. Hernandez, Excited state absorption study in hematoporphyrin IX, J. Fluoresc. 20 (2010) 197–202.
[36] M. Sheik-Bahae, A.A. Said, T.-H. Wei, D.J. Hagan, E.W. Van Stryland, Sensitive measurement of optical nonlinearities using a single beam, IEEE J. Quantum Electron. 26 (1990) 760–769.
[37] L. De Boni, A.A. Andrade, L. Misoguti, C.R. Mendonça, S.C. Zilio, Z-scan measurements using femtosecond continuum generation, Opt. Express 12 (2004) 3921–3927.
[38] L. Misoguti, C.R. Mendonça, S.C. Zilio, Characterization of dynamic optical nonlinearities with pulse trains, Appl. Phys. Lett. 74 (1999) 1531.
[39] (a) L. De Boni, C.J.P. Monteiro, C.R. Mendonça, S.C. Zilio, P.J. Gonçalves, Influence of halogen atoms and protonation on the photophysical properties of sulfonated porphyrins, Chem. Phys. Lett. 633 (2015) 146–151;
(b) E.G. Azenha, A.C. Serra, M. Pineiro, M.M. Pereira, J.S. Melo, L.G. Arnaut, S.J. Formosinho, A.M. Rocha Gonsalves, Heavy-atom effects on metalloporphyrins and polyhalogenated porphyrins, Chem. Phys. 280 (2002) 177–190;
(c) C.J.P. Monteiro, J. Pina, M.M. Pereira, L.G. Arnaut, On the singlet states of porphyrins, chlorins and bacteriochlorins and their ability to harvest red/infrared light, Photochem. Photobiol. Sci. 11 (2012) 1233–1238.
[40] P. Foletto, F. Correa, L. Dornelles, B.A. Iglesias, C.H. da Silveira, P.A. Nogara, J.B.T. da Rocha, M.A.F. Faustino, O.E.D. Rodrigues, A new protocol for the synthesis of new thioaryl-porphyrins derived from 5,10,15,20-Tetrakis(pentafluorophenyl)porphyrin: photophysical evaluation and DNA-Binding interactive studies, Molecules 23 (2018) 2588.
[41] X. Wu, W. Wu, X. Cui, J. Zhao, M. Wu, Preparation of Bodipy–ferrocene dyads and modulation of the singlet/triplet excited state of bodipy via electron transfer and triplet energy transfer, J. Mater. Chem. C 4 (2016) 2843–2853.
[42] T.G.B. Souza, M.G. Vivas, C.R. Mendonça, S. Plunkett, M.A. Filatov, M.O. Senge, L. De Boni, Studying the intersystem crossing rate and triplet quantum yield of meso-substituted porphyrins by means of pulse train fluorescence technique, J. Porphyrins Phthalocyan 20 (2016) 282–291.

[43] M.A. Bakar, N.N. Sergeeva, T. Juillard, M.O. Senge, Synthesis of ferrocenyl porphyrins via suzuki coupling and their photophysical properties, Organometallics 30 (2011) 3225–3228.
[44] M. Drobizhev, A. Karotki, M. Kruk, A. Rebane, Resonance enhancement of two-photon absorption in porphyrins, Chem. Phys. Lett. 355 (2002) 175–182.
[45] Ü. Isci, S.Z. Topal, E. Önal, I. Fidan, S. Berber, V. Ahsen, C. Parejo, Á. Sastre-Santos, F. Dumoulin, Synthesis and characterization of a new meso-tetra-dihydro benzocyclobutacenaphthylene free-base porphyrin, J. Porphyr. Phthalocyan 22 (2018) 173–180.
[46] Z.-B. Liu, Y. Zhu, Y.-Z. Zhu, J.-G. Tian, J.-Y. Zheng, Study on nonlinear spectroscopy of tetraphenylporphyrin and dithiaporphyrin diacids, J. Phys. Chem. B 111 (2007) 14136–14142.
[47] T. Ding, E.A. Alemán, D.A. Modarelli, C.J. Ziegler, Photophysical properties of a series of free-base corroles, J. Phys. Chem. A 109 (2005) 7411–7417.
[48] M. Morone, L. Beverina, A. Abbotto, F. Silvestri, E. Collini, C. Ferrante, R. Bozio, G.A. Pagani, Enhancement of two-photon absorption cross-section and singlet-oxygen generation in porphyrins upon β-functionalization with donor− acceptor substituents, Org. Lett. 8 (2006) 2719–2722.
[49] F. Gotardo, L.H.Z. Cocca, T.V. Acunha, A. Longoni, J. Toldo, P.F.B. Gonçalves, B.A. Iglesias, L. De Boni, Investigating the intersystem crossing rate and triplet quantum yield of Protoporphyrin IX by means of pulse train fluorescence technique, Chem. Phys. Lett. 674 (2017) 48–57.
[50] G. Ao, Z. Xiao, X. Qian, Z. Li, Y. Wang, X. Zhang, Y. Song, Nonlinear optical properties tuning in meso-tetraphenylporphyrin derivatives substituted with donor/acceptor groups in picosecond and nanosecond regimes, Molecules 20 (2015) 5554–5565.
[51] B. Ventura, A.D. Esposti, B. Koszarna, D.T. Gryko, L. Flamigni, Photophysical characterization of free-base corroles, promising chromophores for light energy conversion and singlet oxygen generation, New J. Chem. 29 (2005) 1559–1566.
[52] A.K. Mandal, J.R. Diers, D.M. Niedzwiedzki, G. Hu, R. Liu, E.J. Alexy, J.S. Lindsey, D.F. Bocian, D. Holten, Tailoring panchromatic absorption and excited-state dynamics of tetrapyrrole–chromophore (Bodipy, Rylene) arrays—interplay of orbital mixing and configuration interaction, J. Am. Chem. Soc. 139 (2017) 17547–17564.